Case Studies in Chemical and Environmental Engineering 11 (2025) 101168

Contents lists available at ScienceDirect

Case Studies in Chemical and Environmental Engineering

journal homepage: www.sciencedirect.com/journal/case-studies-in-chemical-and-environmental-engineering

Case Report

Carbon-doped percentage effect on the mechanical properties of nanoporous silicon sample using molecular dynamics simulation

Narinderjit Singh Sawaran Singh [a], Ali B.M. Ali [b], Hawzhen Fateh M. Ameen [c,d], Murtadha M. Al-Zahiwat [e], Soheil Salahshour [f,g,h], Nafiseh Emami [i,*]

[a] Faculty of Data Science and Information Technology, INTI International University, Persiaran Perdana BBN, Putra Nilai, Nilai, 71800, Malaysia
[b] Air Conditioning Engineering Department, College of Engineering, University of Warith Al-Anbiyaa, Karbala, Iraq
[c] Department of Petroleum Technology, Erbil Technology College, Erbil Polytechnic University, Erbil, Kurdistan Region, Iraq
[d] Department of Petroleum Engineering, Knowledge University, Erbil, Iraq
[e] Department of Chemical engineering, College of Engineering, University of Misan, Amarah, Iraq
[f] Faculty of Engineering and Natural Sciences, Istanbul Okan University, Istanbul, Turkey
[g] Faculty of Engineering and Natural Sciences, Bahcesehir University, Istanbul, Turkey
[h] Research Center of Applied Mathematics, Khazar University, Baku, Azerbaijan
[i] Fast Computing Center, Shabihsazan Ati Pars, Tehran, Iran

ARTICLE INFO

Keywords:
Porous materials
Carbon doping
Mechanical properties
Molecular dynamics simulation
Nanoporous

ABSTRACT

Porous materials have attracted considerable attention from researchers due to its many uses in molecular separation, heterogeneous catalysis, absorption technologies, and electronic improvements. These solid materials, often defined by their structural voids, are essential in several sectors. This research investigated the impact of carbon doping on the mechanical characteristics of nanoporous silicon matrices. The use of high-purity silicon doping is very beneficial in the semiconductor industry and is crucial for high-power devices and automotive applications. This study simulates a nanoporous silicon sample by molecular dynamics methods, adding carbon doping at different concentrations. The findings demonstrate that when the carbon doping concentration escalated from 1 % to 30 %, the mechanical resistance of the system decreased correspondingly. The ultimate tensile strength fell from 10.26 to 9.02 GPa. Furthermore, Young's modulus rose from 83.47 to 98.37 GPa. The decline in mechanical stability was associated with a drop in the model's total weight, which had considerable ramifications for industrial applications. Thus, incorporating C-doped nanoporous silicon into real applications not only lowered the weight of target materials but also improved their use.

1. Introduction

Porous materials are distinguished by their high specific surface area, exceptional thermal conductivity, low density, and substantial energy absorption and storage capabilities. These properties render them advantageous for an array of applications [1]. The versatility of these materials in disciplines, such as molecular separation, heterogeneous catalysis, absorption technology, and advancements in optics and electronics sparked extensive scientific interest. In general, a porous material is defined as a solid structure that contains inherent cavities [2–4]. Nanoporous (NP) materials are particularly prevalent in mineral structures and natural and biological systems. Additionally, they are instrumental in a variety of industrial applications [5–7]. The utilization of porous materials was substantially altered by recent developments in nanotechnology and nanoscale manipulation. This transition involved a transition from reliance on natural properties to intentional design in order to provide customized functionalities. Various membrane varieties were developed, allowing for precision control of porosity at the atomic level. This was a prime example. Enabled by sophisticated instruments for atomic and molecular-scale control and production, this precision opened up immense possibilities for utilizing these materials [8–10]. Additionally, the precision with which NP material structures was also applicable at a larger scale. This established these materials as promising candidates for industrial applications, particularly in the pharmaceutical and agricultural sectors [11,12]. Some microporous structures had marginally larger pores, even though NP materials typically had pore diameters below 100 nm. This implied that the 100 nm boundary was not rigorously enforced. A classification system for pore sizes was

* Corresponding author.
E-mail addresses: nafisehemami6672@gmail.com, nafise.emami@iaukhsh.ac.ir (N. Emami).

https://doi.org/10.1016/j.cscee.2025.101168
Received 26 December 2024; Received in revised form 24 February 2025; Accepted 25 February 2025
Available online 25 February 2025
2666-0164/© 2025 The Author(s). Published by Elsevier Ltd. This is an open access article under the CC BY license (http://creativecommons.org/licenses/by/4.0/).

devised by the International Union of Pure and Applied Chemistry in 1985. This system is still frequently consulted today [13]. The first category, microporous materials, comprises structures with pore diameters that are less than 2 nm. The second category, mesoporous materials, encompassed the materials with pore sizes ranging from 2 nm to 50 nm, while the third category, macroporous materials, was defined as those with pore sizes exceeding 50 nm [14–16]. Complex biological structures, such as cell walls, were composed of NP membranes, and NP materials, like many nanostructured substances, occurred naturally in a variety of forms. Zeolites, which were natural NP minerals, were extensively employed in the hydrocarbon industry for decades. Nevertheless, they were now frequently synthesized. In its purest form, silicon was an inadequate electrical conductor; however, the introduction of impurities, a process known as doping, can improve its conductivity, rendering it appropriate for semiconductor applications. For instance, the band gap in graphene and carbon (C)-based structures was effectively reduced by silicon doping, which expands their potential applications in semiconductor technologies. High-purity silicon doping has practical applications in automotive applications and high-power electronics.

The applications of silicon doping were the subject of numerous studies conducted by researchers [17–20]. A study was conducted by Wong et al. [21] to investigate the composition of supramolecular patterns in NP zirconia-silicon catalysts. Using supramolecular patterning at low pH, they effectively synthesized thermally stable mesoporous and microporous zirconium-doped silicon. Materials with homogenous pore diameters and exceedingly high surface areas were produced as a consequence of the incorporation of zirconium into the silicon-based porous framework at levels up to 20 %. The order of these materials was clearly defined. Chu et al. [22] utilized a sol-gel process to create transparent TiO_2/Al_2O_3 NP composite layers that contained a variety of metallic (Ru, Si, Te) and non-metallic (N, C, S) dopants. Their results indicated that the absorption properties of TiO_2 were substantially improved by doping with ruthenium, nitrogen, C, and sulfur. Conversely, the consequences of silicon and tellurium were negligible. Moreover, the photocatalytic activities of NP TiO_2/Al_2O_3 layers under UV light were enhanced by the introduction of nitrogen, C, and sulfur. Conversely, photocatalytic performance was slightly reduced by the doping of ruthenium, silicon, and tellurium. Han et al. [23] employed molecular dynamics (MD) simulations to investigate the mechanical properties of graphene sheets that were doped with silicon and nitrogen atoms. Over a range of doping concentrations from 0 % to 5 %, they analyzed critical metrics, such as Young's modulus, ultimate stress, and strain. Their results suggested that the contamination levels increased in a linear manner, resulting in a decrease in Young's modulus. Silicon doping exhibited more pronounced effects than boron doping, while nitrogen doping had a minimal influence on the mechanical properties of the graphene sheets. Chaus et al. [24] improved the mechanical properties of amorphous C layers by injecting them with silicon in a study. The findings indicated that the residual stresses and surface energy diminished as a consequence of the incorporation of silicon into the amorphous C layers. Zhang et al. [25] investigated the relationship between bond structure and mechanical characteristics in silicon-containing amorphous carbon. Their results indicated that incorporating silicon into the amorphous carbon matrix decreased the extent of sp^2-hybridized carbon bonding and alleviated residual stress. Intriguingly, hardness and elastic modulus decreased as the silicon concentration decreased. Nevertheless, they enhanced with the rising silicon concentration. Rahman et al. [26] performed research on the mechanical properties and fracture behavior of silicon-doped graphene by molecular dynamics simulations. Their findings demonstrated a significant decrease in fracture stress and strain as silicon content increased. At a doping concentration of 5 %, Young's modulus of graphene decreased by 15.5 % in the armchair orientation and by 13.5 % in the zigzag orientation.

Although previous research primarily concentrated on the mechanical properties of various materials, particularly those affected by silicon doping, there was a significant absence of research on the impact of C doping on the mechanical properties of NP silicon matrices. In contrast, the specific implications of C doping in NP silicon remain underexplored, even though doping was demonstrated to enhance or modify mechanical properties in other contexts. This study aimed to investigate the impact of varying percentages of C doping on ultimate strength and Young's modulus of NP silicon to address this disparity. This research improved our comprehension of these materials and underscored their potential for real-world applications that required lightweight and mechanically robust components by conducting a comprehensive analysis through MD simulations. Consequently, this research made a valuable contribution to the body of existing knowledge and addressed practical obstacles in the design and application of materials.

2. MD method

2.1. Simulation details

The mechanical properties of an NP silicon sample (with 10 % porosity) were investigated in this study via MD simulations, with a particular emphasis on the effects of various percentages of C-doped particles. AVOGADRO software [27] was employed to generate a 50 Å NP silicon sample. Carbon atoms were included in the simulation, randomly substituting 1–30 % of silicon atoms with carbon atoms. To induce porosity, 10 % of atoms were randomly removed. The current simulation produced a porous silicon sample by temperature manipulation. The simulation advanced via many NVT equilibration phases, during which "fix nvt" command ensured a constant number of atoms, volume, and temperature via a thermostat. The phases included a methodical elevation of temperature, commencing at 300 K and ascending to 600 K, subsequently followed by a slow decrement to 500 K, 400 K, and ultimately returning to 300 K. This thermal variation was intended to alter material's structure, with heating likely resulting in expansion and subsequent cooling inducing the creation of voids or holes inside the silicon sample. The periodic boundary conditions are applied in all directions. Tersoff potential modeled the interaction between silicon and carbon atoms, while a conjugate gradient method minimized the system's energy. A time step of 1 fs was consistently used for the simulations. The equilibrium phase was first examined using an NVT ensemble over 100,000 time steps, followed by an evaluation of the mechanical properties of the simulated structure. Fig. 1 depicts a schematic depiction of the modeled NP silicon sample. Also, MD simulation details in present work are given in Table 1.

The results of this study were categorized into two parts. Initially, before evaluating the mechanical properties of porous silicon samples, essential physical parameters, including temperature and kinetic energy, were analyzed to attain equilibrium and comprehend the atomic behavior of the nanostructure. The mechanical properties of the silicon sample were then reported based on the simulation findings.

2.2. Equilibrium investigation of nanostructure

Establishing equilibrium in atomic systems was crucial given the specified initial conditions. Fig. 2 depicts the temperature progression of the simulated nanostructure across 100,000-time steps. Initially, temperature variations were noted as the system adapted to the established settings. As the simulation advanced, a distinct stability at 300 K was attained, indicating that the system had achieved thermal equilibrium. This stabilization was essential since it indicated an equilibrium between kinetic and potential energy inside the system, implying that atomic interactions reached a stable state. The convergence of temperature indicated a substantial reduction in the mobility of carbon atoms inside the silicon matrix. As the temperature equilibrated, atomic vibrations decreased, resulting in a more organized atomic configuration.

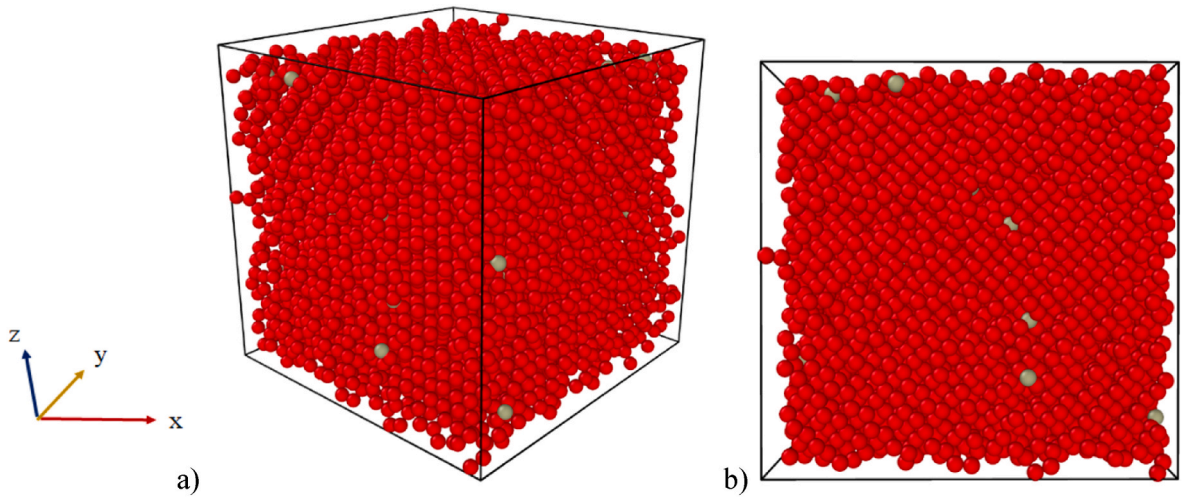

Fig. 1. A view of the simulated structure from a) perspective and b) side view in the presence of 1 % C-doped.

Table 1
MD simulation details in present work.

Computational Parameter	Setting
Computational Box Length	50 × 50 × 50 Å^3
Number of Atoms	7238
Boundary Condition	P P P
Thermostat	Nose-Hoover
Ensembles	NVT
Minimization	cg algorithm
Time Step	1 fs
Initial Temperature	300 K
Damping Ratio for Temperature	0.1
Time-steps	100,700

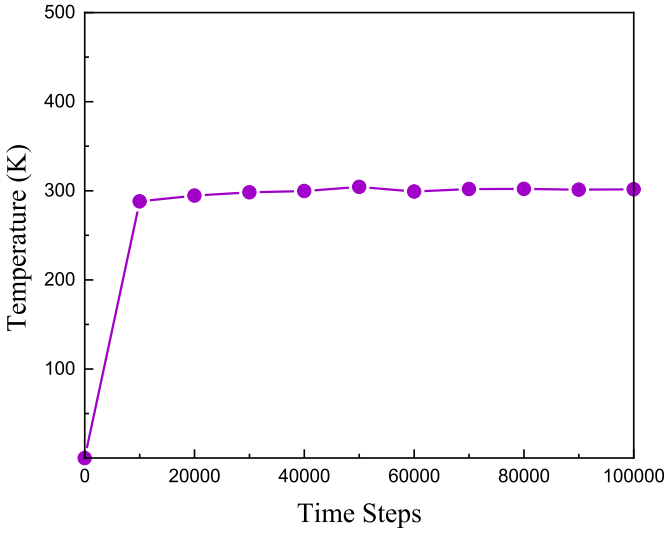

Fig. 2. Temperature variations vs. time steps.

This diminished mobility was crucial for preserving structural integrity. The observed stability was due to the meticulous selection of potential functions used in the LAMMPS simulation framework, which precisely represented interatomic interactions. Utilizing suitable potentials guaranteed that silicon and carbon atoms exhibited realistic behavior in simulated environments, hence enabling an accurate depiction of their structural properties and validating that selected parameters appropriately encapsulate the dynamics of the material system.

The relationship between atomic motion and temperature was essential, as shown in the preceding section. The kinetic energy of the nanostructure stabilized at a steady state of 282.24 eV after 100,000-time steps, as seen in Fig. 3. This stabilization was associated with diminished fluctuations in the system, affirming the thermodynamic equilibrium of the nanostructure. It corroborated previous research, highlighting the precise characterization of atomic nanostructures and associated interatomic potentials [28,29]. The stability of interatomic distances in nanoparticles directly stemmed from this equilibrium, guaranteeing uniform kinetic energy values in the atomic samples.

2.3. *Mechanical test*

Following equilibration, the mechanical characteristics of the NP silicon sample were examined using a stress-strain curve. In this phase, the C matrix was elongated along with the X-axis at a tensile rate of 1 s^{-1} (see Fig. 4). The variation in Young's modulus and ultimate strength was assessed throughout the structure. This mechanical process resulted in a decline in mechanical characteristics inside the MD box. The physical stability of modeled porous materials was assessed by molecular dynamics simulation parameters, including the atomic modeling methodology and the selected interatomic potential.

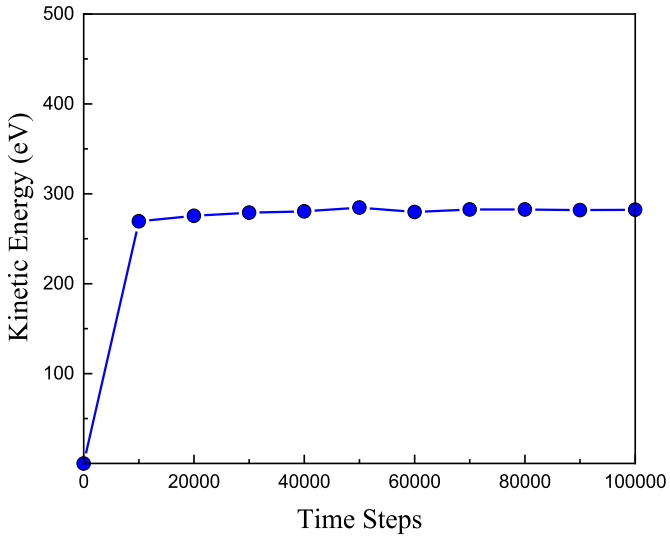

Fig. 3. Kinetic energy variations vs. time steps.

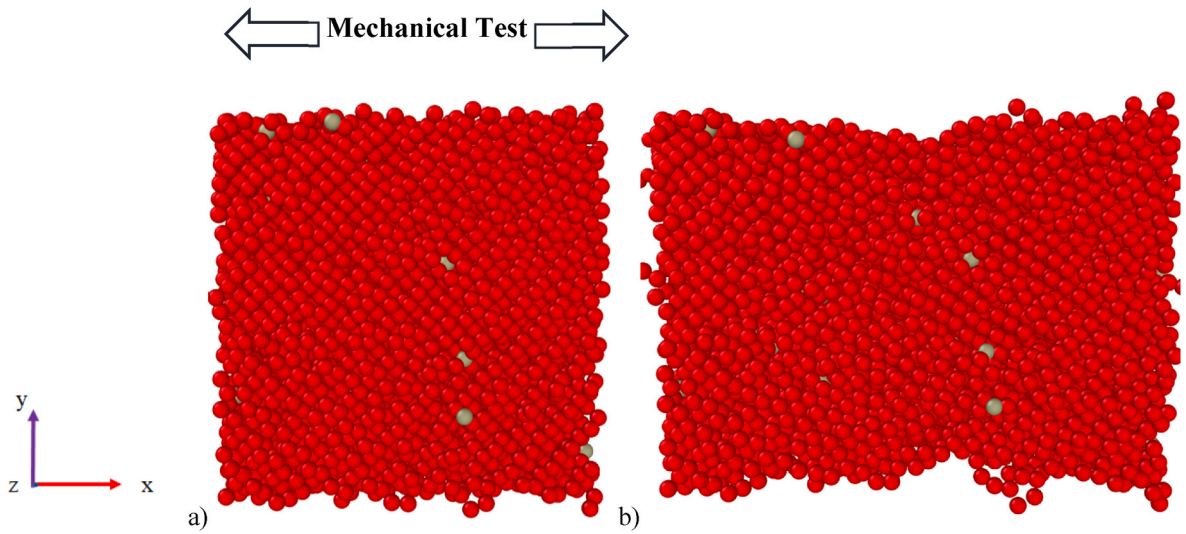

Fig. 4. A view of the mechanical test at a) first and b) final time steps.

3. Results and discussion

The findings of our computational research, shown in Fig. 5, indicate that the ultimate strength of the doped silicon porous sample was 10.49 GPa. The computed Young's modulus was 83.47 GPa. The alignment of our results with prior research emphasized the dependability of our computational method and confirmed the efficacy of our models in forecasting material behavior under diverse doping conditions [30,31].

Fig. 6 depicts the hardness of the NP silicon sample with 1 % carbon doping. Toughness quantifies a material's capacity to absorb energy and undergo plastic deformation without breaking, determined by calculating the area under the stress-strain curve. This region denoted the total energy per unit volume that a material can endure before failure, including elastic and plastic deformation. An increased area signified enhanced toughness, enabling the material to endure more stress and strain before breakdown. Toughness was crucial in applications exposed to dynamic loads or impacts since it signified robustness and durability. Comprehending toughness via a stress-strain curve enabled engineers to choose materials capable of enduring operating pressures without failure.

Fig. 7 depicts the silicon porous sample with carbon doping levels between 5 % and 30 %, demonstrating its physical stability during an equilibration procedure of 100,000-time steps, an essential criterion for prospective industrial applications. The stability affirmed the structural

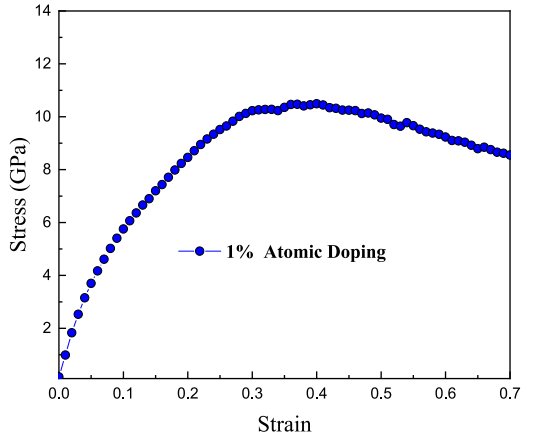

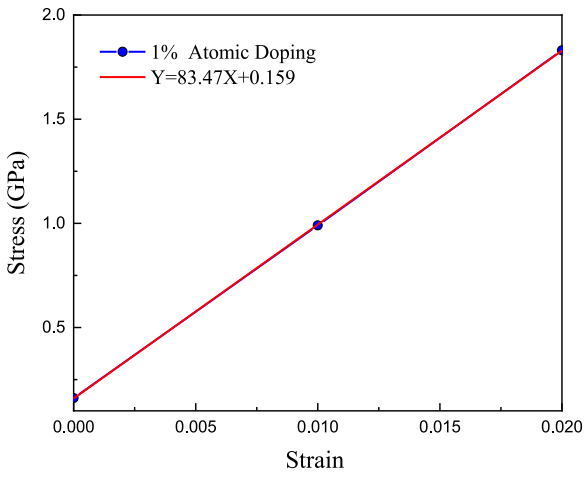

Fig. 5. a) Stress-strain curve and b) linear fitted curve of NP silicon sample in 1 % C doping.

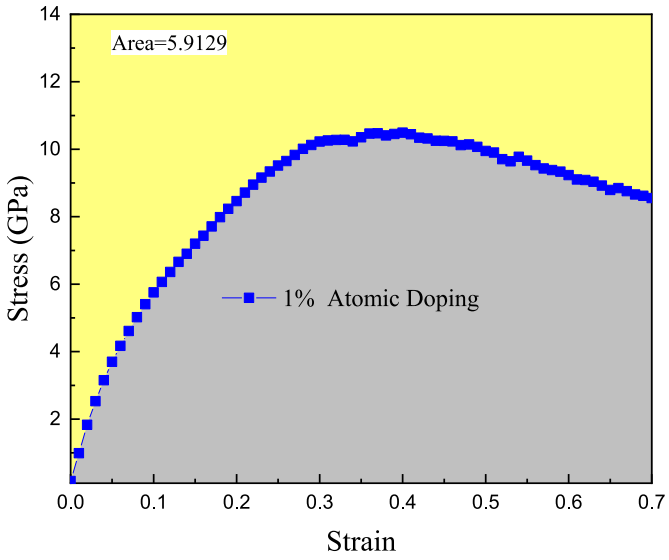

Fig. 6. Toughness of NP silicon sample in 1 % C doping.

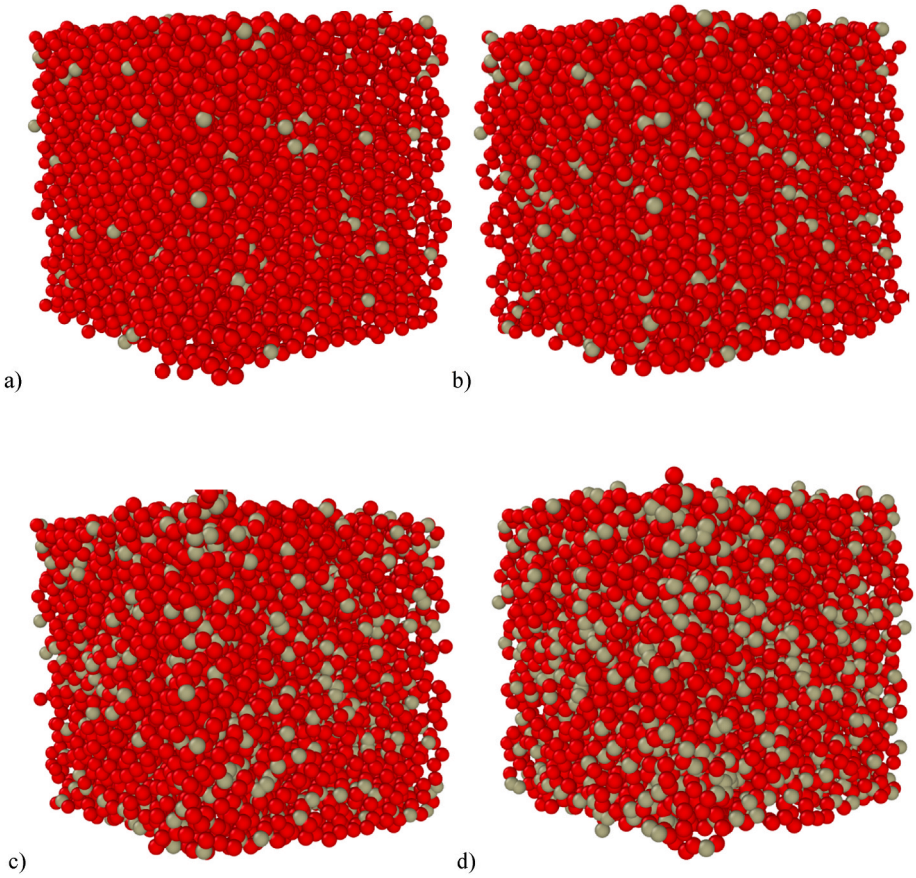

Fig. 7. The atomic representation of NP silicon sample in the presence of a) 5 %, b) 10 %, c) 20 %, and d) 30 % of C doping.

integrity of doped porous matrices and indicated their capacity to endure real-world operating settings, rendering them appropriate candidates for diverse applications in areas, such as catalysis, filtration, and lightweight structural materials. Upon confirming physical stability in the MD simulation environment, we established mechanical deformation parameters to evaluate the samples' reaction to stress. Examining the mechanical performance of these doped structures was vital for comprehending their behavior under stress, which informed their practical use in industrial contexts where mechanical durability is imperative. By examining the mechanical reaction of these stable combinations, we may enhance their design for particular applications, assuring compliance with performance criteria while preserving stability in operating environments.

The mechanical outputs at this phase are shown in Fig. 8. The findings revealed a significant reduction in the mechanical strength of the modeled matrix with an increase in the C doping ratio. The decrease in strength was ascribed to augmented interatomic distances inside the porous materials, negatively impacting their structural integrity. The incorporation of carbon atoms into the silicon sample altered the atomic interactions, resulting in a reduction of attractive forces that maintained the structure. This process arose from the degradation of covalent connections between the silicon framework and dopant atoms, resulting in a less cohesive structure. This response highlighted the need to adjust the doping ratio to enhance characteristics like porosity and functionalization while preserving sufficient mechanical strength for industrial applications. Comprehending these linkages was essential for customizing materials for particular applications, guaranteeing optimal performance without jeopardizing structural integrity.

As a function of the C doping ratio, Fig. 9 illustrates the variation of ultimate strength in a porous silicon sample. In particular, ultimate strength decreased from 10.26 GPa to 9.02 GPa as the contamination ratio increased from 10 % to 30 %. The utmost stress that a material can withstand before it failed was referred to as its ultimate strength. The ultimate strength decrease that occurred as carbon supplementation increased can be attributed to a variety of factors. First and foremost, regular silicon-silicon bonding networks can be disrupted by carbon atoms, resulting in weaker bonds than the strong covalent bonds found in pure silicon. This disruption may reduce the load-bearing capacity of the material. Furthermore, at elevated doping levels, carbon may induce phase separation or clusters within the silicon sample, which serve as stress concentrators that contribute to premature failure. Additionally, the material may experience an overall deterioration as a consequence of the inherent nanoporous structure becoming more susceptible to these modifications.

Fig. 10 shows the Young's modulus changes of NP silicon sample as a function of C doping ratio. This parameter rose when calculating Young's modulus in 0–0.02 strain range. The observed rise in Young's modulus with carbon doping indicated increased stiffness in the material. This improvement may be due to the stiffening impact of carbon atoms, which generated new covalent bonding contacts that helped retain the structural integrity of the silicon framework despite its porosity. Furthermore, carbon doping may improve cross-linking within the silicon sample, increasing load-bearing capacity and leading to a greater Young's modulus. Furthermore, the presence of carbon may limit the mobility of dislocations and faults, leading to a stiffer reaction to applied stresses. In general, the kind and quantity of dopant had a considerable impact on bonding properties and microstructure, resulting in variations in how the material reacted to applied stresses [32]. When an external force was applied to the doped material, the stress and strain did not spread evenly across the sample. Instead, certain places had larger stress concentrations than others owing to variables, such as dopant atom arrangement, porosity, and material microstructure [33].

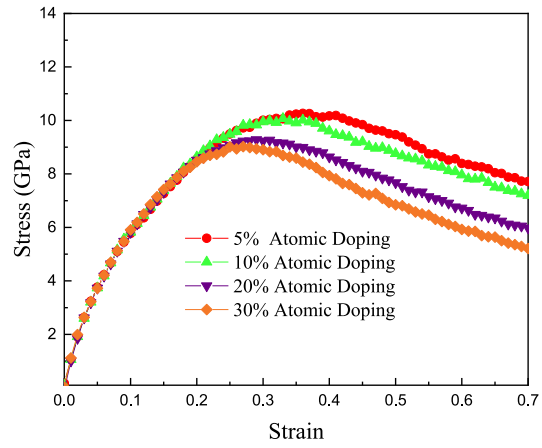

a)

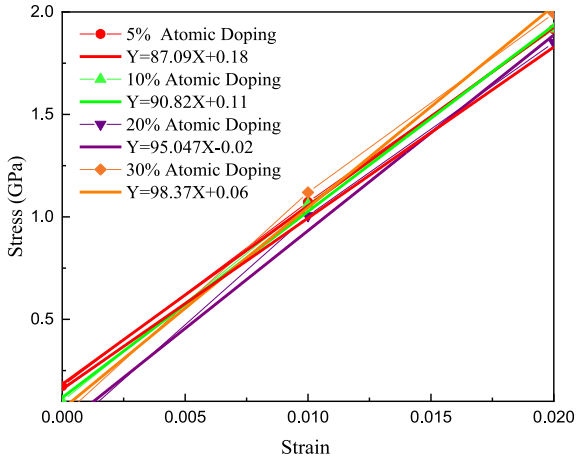

b)

Fig. 8. a) Stress-strain and b) Young's modulus of NP silicon system in the presence of C dopes with various ratios.

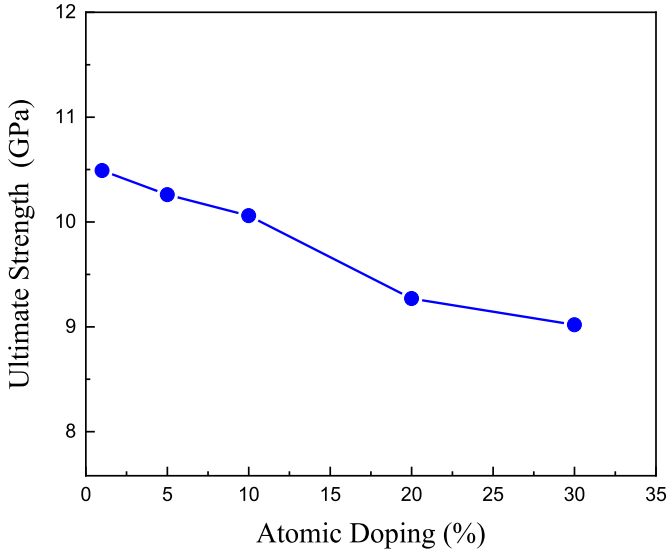

Fig. 9. The ultimate strength changes of the NP silicon sample as a function of C doping ratio.

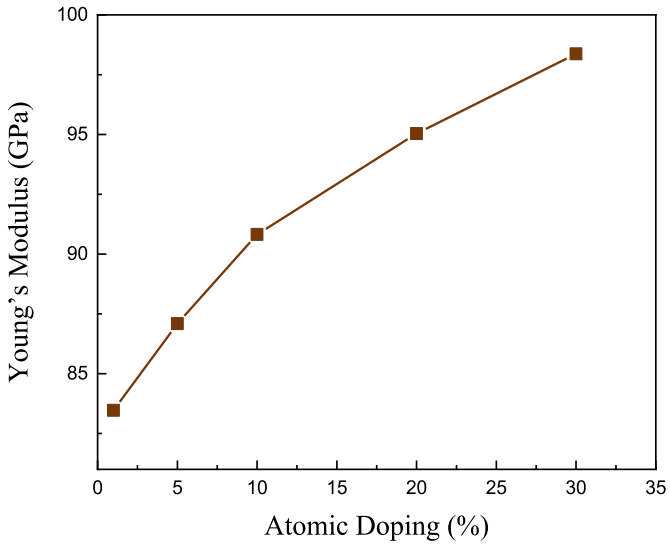

Fig. 10. Young's modulus changes of NP silicon sample as a function of C doping ratio.

Even if the material had a high overall Young's modulus, its non-uniform stress distribution might cause localized deformation or failure6. For example, whereas carbon doping might enhance overall stiffness, specific places may still fracture or give under severe stress [34]. Additional numerical results relevant to this section are summarized in Table 2.

The durability of the NP silicon sample is depicted in Fig. 11 as a function of the C doping ratio. The findings suggested that the durability of the material decreased as the level of C contamination increased. As carbon doping increased, the ductility of nanoporous silicon (NP silicon) samples decreased from 5.912 to 4.754 eV/Å^3, primarily as a result of the disruption of the silicon bonding network. The introduction of carbon into the silicon matrix disrupted the strong covalent bonds that silicon typically forms, resulting in weakened bonding environments that diminished the material's capacity to absorb energy before fracturing. Furthermore, the formation of carbon-rich clusters or phase separation may result from high levels of carbon doping, which serve as stress concentrators. Crack initiation and propagation were facilitated by these localized vulnerabilities, which further reduced durability. Additionally, the porosity of the silicon matrix may be impacted by the introduction of carbon, which could result in a reduction in the effective load-bearing area and an increase in the number of defects. The material's energy absorption capacity was restricted by this reduction in structural integrity, resulting in lower toughness values. Additionally, the material's capacity to endure plastic deformation may be limited by carbon modification, which may impede dislocation movement within the silicon microstructure. This limitation led to a more brittle response to stress, which contributed to an overall decrease in resilience as the carbon concentration increased.

Table 2
The ultimate strength, Young's modulus, and Toughness variation of NP silicon sample as a function of the C doping ratio.

Atomic Doping (%)	Ultimate Strength (GPa)	Young's Modulus (GPa)	Toughness (eV/Å^3)
1	10.49	83.47	5.912
5	10.26	87.09	5.703
10	10.06	90.82	5.530
20	9.27	95.04	5.038
30	9.02	98.37	4.754

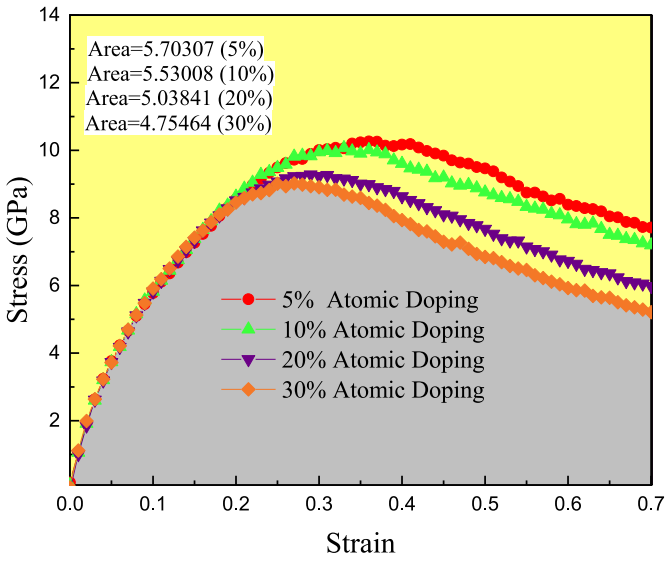

Fig. 11. The Toughness changes of NP silicon sample as a function of C doping ratio.

4. Conclusion

This research investigated the effects of carbon (C) doping on the atomic and mechanical performance of nanoporous (NP) silicon systems using MD simulations. The key findings are summarized as follows.

- The physical stability of C-doped NP silicon samples was corroborated by temperature and kinetic energy calculations, which converged to 300 K and 282.24 eV, respectively, after 100,000-time steps. This suggested that simulation configuration and parameters produced robust systems that were appropriate for additional mechanical testing.
- The ultimate strength of NP silicon samples decreased from 10.26 GPa to 9.02 GPa as the carbon contamination ratio increased.
- Young's modulus increased from 83.47 GPa to 98.37 GPa as the carbon contamination ratio increased.

The carbon doping ratio significantly affects the mechanical properties and stability of the nanostructured silicon samples. This tunability enables customized modifications to satisfy particular demands in diverse industrial applications where stiffness and strength are essential factors.

CRediT authorship contribution statement

Narinderjit Singh Sawaran Singh: Formal analysis, Data curation, Conceptualization, Supervision, Validation, Visualization, Writing – original draft, Writing – review & editing. **Ali B.M. Ali:** Formal analysis, Data curation, Conceptualization, Supervision, Validation, Visualization, Writing – original draft, Writing – review & editing. **Hawzhen Fateh M. Ameen:** Formal analysis, Data curation, Conceptualization, Supervision, Validation, Visualization, Writing – original draft, Writing – review & editing. **Murtadha M. Al-Zahiwat:** Formal analysis, Data curation, Conceptualization, Supervision, Validation, Visualization, Writing – original draft, Writing – review & editing. **Soheil Salahshour:** Formal analysis, Data curation, Conceptualization, Supervision, Validation, Visualization, Writing – original draft, Writing – review & editing. **Nafiseh Emami:** Formal analysis, Data curation, Conceptualization, Supervision, Validation, Visualization, Writing – original draft, Writing – review & editing.

Declaration of competing interest

The authors declare that they have no known competing financial interests or personal relationships that could have appeared to influence the work reported in this paper.

Appendix

A. MD Simulation

MD simulation is a computational modeling technique that enables the study of atomic and molecular interactions over time, based on the principles of classical physics. This approach allows for the visualization of atomic movements, offering insights into their dynamic behavior. Given the large number of particles in molecular systems, traditional analytical methods for deriving properties of such complex multi-particle systems can be extremely challenging, if not unfeasible. To overcome this limitation, MD simulations utilize numerical methods for analysis. Central to the MD simulation method are Newton's equations of motion, which govern particle behavior.

The trajectory of each particle within the simulation is determined by solving these equations, allowing for the calculation of their positions and velocities over time. The force acting on particle i is mathematically represented by the following equation [35,36]:

$$F_i = m_i a_i = m_i \frac{d^2 r_i}{dt^2} \tag{a-1}$$

In Eq. (a-1), m_i denotes the mass of the particle, a_i indicates the particle's acceleration, and r_i is a vector that defines the particle's position concerning a reference frame. The force exerted on the particle is related to the potential function, which can be expressed in the following form as described in Eq. (2) [35,36]:

$$F_i = -\nabla_i U \tag{a-2}$$

By integrating the aforementioned relationships, a formula is derived that describes the position of the particles in terms of the potential function:

$$-\frac{dU}{dr_i} = m_i \frac{d^2 r_i}{dt^2} \tag{a-3}$$

Numerous numerical methods exist for calculating integrals, with the finite difference method being particularly significant. The velocity-Verlet algorithm, based on the finite difference method, is one of the most efficient approaches for numerically integrating equations of motion, offering high accuracy. This algorithm can be articulated using the following equations [37–39]:

$$r_i\ (\mathrm{t}+\Delta\mathrm{t}) = 2\ r_i(t) - r_i(t-\Delta t) + \left(\frac{d^2 r_i}{dt^2}\right)(\Delta t)^2 \tag{a-4}$$

In Eq. (4), $r_i\ (\mathrm{t}+\Delta\mathrm{t})$ the notation indicates the particle's position at subsequent time intervals. The particle's velocity and acceleration at the next time step $(\mathrm{t}+\Delta\mathrm{t})$ are calculated using the following relations:

$$v_i(t+\Delta t) = v_i(t) + \Delta t\ a_i(t) + \frac{\Delta t\ (a_i\ (t) + a_i(t+\Delta t))}{2} \tag{a-5}$$

$$a_i(t+\Delta t) = \frac{F_i\ (t+\Delta t)}{m_i} \tag{a-6}$$

Characterizing the potential function and interparticle forces is essential for this method. MD simulations require a potential function that accurately describes the interactions among the system's components, providing a comprehensive view of particle interactions. In this study, the Tersoff potential function is used to define the interactions between carbon atoms within the simulation framework. The mathematical formulation representing the Tersoff potential function is as follows [40]:

$$E = \frac{1}{2}\sum_i \sum_{j\neq i} V_{ij} \tag{a-7}$$

$$V_{ij} = f_C(r_{ij})\left[f_R(r_{ij}) + b_{ij} f_A(r_{ij})\right] \tag{a-8}$$

$$\mathrm{f}_C(r) = \begin{cases} 1 & r < R - D \\ \frac{1}{2} - \frac{1}{2}sin\left(\frac{\pi}{2}\frac{r-R}{D}\right) & R - D < r < R + D \\ 0 & r > R + D \end{cases} \tag{a-9}$$

In Eq. (8), $\mathrm{f_R}$ represents the interaction among absorbing particles, which can be expressed in a general form as follows:

$$f_R(r) = A\ \exp(-\lambda_1 r) \tag{a-10}$$

Additionally, $\mathrm{f_A}$ denotes the repulsive interaction among particles, which can be described by the following general form:

$$f_A(r) = -B\ \exp(-\lambda_2 r) \tag{a-11}$$

In the equations presented, the constants A and B represent the potential coefficients that are specific to the structures under investigation. The term $\mathrm{b_{ij}}$ as defined in Eq. (12), is determined by the following relationship:

$$b_{ij} = \left(1 + \beta^n {\varphi_{ij}}^n\right)^{-\frac{1}{2n}} \tag{a-12}$$

$$\varphi_{ij} = \sum_{k\neq ij} f_C(r_{ik}) g(\theta_{ijk}) exp\left[\lambda_3^m \left(r_{ij} - r_{ik}\right)^m\right] \tag{a-13}$$

The function of g(θ) is associated with the angle formed among particles i and j, as well as the angle among particles i and k.

Data availability

No data was used for the research described in the article.

References

[1] M.F. Ashby, T. Evans, N.A. Fleck, J. Hutchinson, H. Wadley, L. Gibson, Metal Foams: a Design Guide, Elsevier, 2000.

[2] K. Kaneko, Determination of pore size and pore size distribution: 1. Adsorbents and catalysts, J. Membr. Sci. 96 (1–2) (1994) 59–89.

[3] D.M. Antonelli, J.Y. Ying, Mesoporous materials, Curr. Opin. Colloid Interface Sci. 1 (4) (1996) 523–529.

[4] K. Ajay, M. Dinesh, G. Byatarayappa, M. Radhika, N. Kathyayini, H. Vijeth, Electrochemical investigations on low cost KOH activated carbon derived from orange-peel and polyaniline for hybrid supercapacitors, Inorg. Chem. Commun. 127 (2021) 108523.

[5] W. Yantasee, R.D. Rutledge, W. Chouyyok, V. Sukwarotwat, G. Orr, C.L. Warner, M.G. Warner, G.E. Fryxell, R.J. Wiacek, C. Timchalk, Functionalized nanoporous silica for the removal of heavy metals from biological systems: adsorption and application 2 (10) (2010) 2749–2758.

[6] S.P. Mishra, S. Dutta, A.K. Sahu, K. Mishra, P. Kashyap, Potential application of nanoporous materials in biomedical field, in: Nanopores, IntechOpen, 2021.

[7] H. Sayadi, Recent Advances in Properties and Applications of Nanoporous Materials and Porous Carbons, 2022, pp. 1–25.

[8] A. Burggraaf, K. Keizer, B.A. Van Hassel, in: Ceramic Nanostructure Materials, Membranes and Composite Layers, vol. 32, 1989, pp. 771–782.

[9] Y. Ohta, K. Akamatsu, T. Sugawara, A. Nakao, A. Miyoshi, S.-I. Nakao, Development of pore size-controlled silica membranes for gas separation by chemical vapor deposition 315 (1–2) (2008) 93–99.

[10] B.N. Nair, T. Yamaguchi, T. Okubo, H. Suematsu, K. Keizer, S.-I. Nakao, Sol-gel synthesis of molecular sieving silica membranes, J. Membr. Sci. 135 (2) (1997/11/26/, 1997) 237–243.

[11] A. Bernardos Bau, L. Kourimska, Applications of mesoporous silica materials in food: a review 31 (2) (2013) 99–107.

[12] E.P. Favvas, in: Hybrid Porous Nanomaterials for Energy and Environment, vol. 14, MDPI, 2022, p. 2471.

[13] T. Mays, A new classification of pore sizes, Characterization of Porous Solids VII 160 (2007) 57–62.

[14] B. Li, H. Xiong, Y. Xiao, Progress on synthesis and applications of porous carbon materials, Int. J. Electrochem. Sci. 15 (2) (2020) 1363–1377.

[15] T. Kesavan, T. Partheeban, M. Vivekanantha, M. Kundu, G. Maduraiveeran, M. Sasidharan, Hierarchical nanoporous activated carbon as potential electrode materials for high performance electrochemical supercapacitor, Microporous Mesoporous Mater. 274 (2019) 236–244.

[16] S. De, A.M. Balu, J.C. Van Der Waal, R. Luque, Biomass-derived porous carbon materials: synthesis and catalytic applications, ChemCatChem 7 (11) (2015) 1608–1629.

[17] A.R. Albooyeh, A. Dadrasi, A.H. Mashhadzadeh, Effect of point defects and low-density carbon-doped on mechanical properties of BNNTs: a molecular dynamics study, Mater. Chem. Phys. 239 (2020/01/01/, 2020) 122107.

[18] L. Zhang, M. Kai, X. Chen, in: Si-doped Graphene in Geopolymer: its Interfacial Chemical Bonding, Structure Evolution and Ultrastrong Reinforcing Ability, vol. 109, 2020 103522.

[19] J.-I. Kim, Y.-J. Jang, J. Kim, J. Kim, Effects of silicon doping on low-friction and high-hardness diamond-like carbon coating via filtered cathodic vacuum arc deposition 11 (1) (2021) 1–13.

[20] R. Zarei Moghadam, H. Rezagholipour Dizaji, M. Ehsani, Modification of optical and mechanical properties of nitrogen doped diamond-like carbon layers 30 (22) (2019) 19770–19781.

[21] M.S. Wong, H.C. Huang, J.Y. Ying, Supramolecular-templated synthesis of nanoporous Zirconia−Silica catalysts, Chem. Mater. 14 (5) (2002/05/01, 2002) 1961–1973.
[22] S.-Z. Chu, S. Inoue, K. Wada, D. Li, J. Suzuki, Fabrication and photocatalytic characterizations of ordered nanoporous X-doped (X = N, C, S, Ru, Te, and Si) TiO2/Al2O3 films on ITO/glass, Langmuir 21 (17) (2005/08/01, 2005) 8035–8041.
[23] T. Han, Y. Luo, C. Wang, Effects of SI, N and B doping on the mechanical properties of graphene sheets 28 (6) (2015) 618–625.
[24] A.S. Chaus, X.H. Jiang, P. Pokorný, D.G. Piliptsou, A.V. Rogachev, Improving the mechanical property of amorphous carbon films by silicon doping, Diam. Relat. Mater. 82 (2018/02/01/, 2018) 137–142.
[25] S.-E. Ong, S. Zhang, H. Du, D. Sun, Relationship between bonding structure and mechanical properties of amorphous carbon containing silicon, Diam. Relat. Mater. 16 (8) (2007/08/01/, 2007) 1628–1635.
[26] M.H. Rahman, S. Mitra, M. Motalab, P. Bose, Investigation on the mechanical properties and fracture phenomenon of silicon doped graphene by molecular dynamics simulation 10 (52) (2020) 31318–31332.
[27] M.D. Hanwell, D.E. Curtis, D.C. Lonie, T. Vandermeersch, E. Zurek, G.R. Hutchison, Avogadro: an advanced semantic chemical editor, visualization, and analysis platform, J. Cheminf. 4 (2012) 1–17.
[28] A. Mosavi, M. Hekmatifar, A.a. Alizadeh, D. Toghraie, R. Sabetvand, A. Karimipour, The molecular dynamics simulation of thermal manner of Ar/Cu nanofluid flow: the effects of spherical barriers size, J. Mol. Liq. 319 (2020) 114183.
[29] A. Asgari, Q. Nguyen, A. Karimipour, Q.-V. Bach, M. Hekmatifar, R. Sabetvand, Investigation of additives nanoparticles and sphere barriers effects on the fluid flow inside a nanochannel impressed by an extrinsic electric field: a molecular dynamics simulation, J. Mol. Liq. 318 (2020) 114023.
[30] V. Ivashchenko, P. Turchi, V. Shevchenko, Simulations of the mechanical properties of crystalline, nanocrystalline, and amorphous SiC and Si, Phys. Rev. B 75 (8) (2007) 085209.
[31] Y.V. Milman, I. Gridneva, A. Golubenko, Construction of stess-strain curves for brittle materials by indentation in a wide temperature range, Sci. Sinter. 39 (1) (2007) 67–75.
[32] S.-R.G. Christopoulos, E.N. Sgourou, A. Chroneos, C.A. Londos, Carbon-isovalent dopant pairs in silicon: a density functional theory study, Appl. Sci. 14 (10) (2024) 4194.
[33] M. Hekmatifar, D. Toghraie, R. Sabetvand, S. Esmaeili, Effect of electric field magnitude on the mechanical behavior of silicon-doped nanoporous carbon matrix by molecular dynamics method, Progress in Physics of Applied Materials 2 (2) (2022) 157–164.
[34] S.B. Olou'ou Guifo, J.E. Mueller, D. Henriques, T. Markus, Effects of carbon impurities on the performance of silicon as an anode material for lithium ion batteries: an ab initio study, AIP Adv. 12 (3) (2022).
[35] D.C. Rapaport, D.C.R. Rapaport, The Art of Molecular Dynamics Simulation, Cambridge university press, 2004.
[36] B.J. Alder, T.E. Wainwright, "Studies in molecular dynamics, I. General method 31 (2) (1959) 459–466.
[37] L. Verlet, "Computer" experiments" on classical fluids. I, Thermodynamical properties of Lennard-Jones molecules 159 (1) (1967) 98.
[38] W.C. Swope, H.C. Andersen, P.H. Berens, K.R. Wilson, A computer simulation method for the calculation of equilibrium constants for the formation of physical clusters of molecules: application to small water clusters 76 (1) (1982) 637–649.
[39] E. Hairer, C. Lubich, G. Wanner, in: Geometric Numerical Integration Illustrated by the Störmer–Verlet Method, vol. 12, 2003, pp. 399–450.
[40] J. Tersoff, New empirical approach for the structure and energy of covalent systems 37 (12) (1988) 6991.